

Rocksalt SnS and SnSe: Native topological crystalline insulatorsYan Sun,^{1,2,3} Zhicheng Zhong,⁴ Tomonori Shirakawa,^{2,5,6} Cesare Franchini,³ Dianzhong Li,¹ Yiyi Li,¹ Seiji Yunoki,^{2,5,6,7} and Xing-Qiu Chen^{1,*}¹*Shenyang National Laboratory for Materials Science, Institute of Metal Research, Chinese Academy of Sciences, Shenyang 110016, China*²*Computational Condensed Matter Physics Laboratory, RIKEN, Wako, Saitama 351-0198, Japan*³*Computational Materials Physics, Faculty of Physics, University of Vienna, Sensengasse 8/7, A-1090 Vienna, Austria*⁴*Institute of Solid State Physics, Vienna University of Technology, 1040 Vienna, Austria*⁵*CREST, Japan Science and Technology Agency (JST), Kawaguchi, Saitama 332-0012, Japan*⁶*Computational Materials Science Research Team, RIKEN Advanced Institute for Computational Science (AICS), Kobe, Hyogo 650-0047, Japan*⁷*Computational Quantum Matter Research Team, RIKEN Center for Emergent Matter Science (CEMS), Wako, Saitama 351-0198, Japan*

(Received 16 August 2013; revised manuscript received 22 November 2013; published 19 December 2013)

Unlike time-reversal topological insulators, surface metallic states with Dirac cone dispersion in the recently discovered topological crystalline insulators (TCIs) are protected by crystal symmetry. To date, TCI behaviors have been observed in SnTe and the related alloys $\text{Pb}_{1-x}\text{Sn}_x\text{Se/Te}$, which incorporate heavy elements with large spin-orbit coupling (SOC). Here, by combining first-principles and *ab initio* tight-binding calculations, we report the formation of a TCI in relatively lighter rocksalt SnS and SnSe. This TCI is characterized by an even number of Dirac cones at the high-symmetry (001), (110), and (111) surfaces, which are protected by the reflection symmetry with respect to the $(\bar{1}10)$ mirror plane. We find that both SnS and SnSe have an intrinsically inverted band structure even without the SOC and the SOC is necessary only to open the bulk band gap. The bulk band gap evolution upon volume expansion reveals a topological transition from an ambient pressure TCI to a topologically trivial insulator. Our results indicate that the SOC alone is not sufficient to drive the topological transition.

DOI: [10.1103/PhysRevB.88.235122](https://doi.org/10.1103/PhysRevB.88.235122)

PACS number(s): 73.20.At, 71.20.-b, 71.70.Ej

I. INTRODUCTION

Since the discovery of Z_2 topological insulators (TIs),^{1,2} band topological properties in condensed matter physics have attracted increasing interest as a new physical paradigm, which also shows great promise for potentially revolutionary applications in quantum computing and spintronics. TIs possess a nontrivial time-reversal Z_2 topological invariant and the topological characteristics are manifested by the presence of an odd number of linearly dispersing Dirac cones at the crystal surfaces. These surface metallic states are due to large spin-orbit coupling (SOC) and are protected by time-reversal symmetry.^{1,2}

In 2011, Fu proposed a theoretical model for an alternative class of topological states, named topological crystalline insulators (TCIs), in which the gapless surface states are protected not by time-reversal symmetry but by crystal symmetry.^{3,4} Up to now, the only reported TCIs are the narrow band gap semiconductor SnTe and the related alloys $\text{Pb}_{1-x}\text{Sn}_x\text{Se/Te}$.⁵⁻⁹ Very recently, Barone *et al.* have theoretically predicted that a suitable combination of applied pressure and alloying can turn rocksalt lead chalcogenides, such as PbSe, PbTe, and PbS, into TCIs.¹⁰ The most prominent feature of this class of TCIs is the presence of an even, not odd as in TIs, number of Dirac cones, which lie on surface terminations oriented perpendicular to the mirror symmetry planes. It is shown that the necessary conditions for the band inversions to occur in all these TCIs are (i) a strongly asymmetric hybridization between cation (anion) s and anion (cation) p states and (ii) a sizable SOC strength, similarly in time-reversal TIs.¹¹⁻¹⁸ Large SOC is recognized to be a crucial ingredient to form possible TCIs also in pyrochlore oxides $A_2\text{Ir}_2\text{O}_7$, where A is a rare-earth element.¹⁹ However, TCIs can be considered as the counterpart of TIs in materials

without SOC.³ Thus, it is of fundamental importance to seek a manifestation of the nontrivial crystalline topology in materials composed of constituents with lighter mass and thus smaller SOC, for which the SOC effect is detached from the formation of TCIs.

In this paper, through first-principles calculations along with Wannier functions based *ab initio* tight-binding (TB) modeling, we report that rocksalt SnS and SnSe are both TCIs in their native phase without any alloying or applied strain/pressure. We find that their inverted band order is induced by chemical bonding and crystal field, whereas the SOC effect is only to open the bulk band gap. This nontrivial topological state is substantiated by the emergence of an even number of Dirac cones at the high-symmetry crystal surfaces perpendicular to the $(\bar{1}10)$ mirror symmetry plane. We also demonstrate that a topological transition occurs to a trivial insulator upon volume expansion.

The rest of the paper is organized as follows. Numerical methods employed are briefly described in Sec. II, where the total energies for two different structure phases of bulk SnS and SnSe are also compared. The numerical results follow in Sec. III. In Sec. III A, we first show the bulk energy band structures with and without SOC and discuss the topological properties of SnS and SnSe. Then the surface band structures are discussed in Sec. III B, providing evidence of the topologically nontrivial nature of SnS and SnSe. Finally, the conclusions of this paper are given in Sec. IV.

II. METHODS

First-principles calculations based on density functional theory (DFT) are performed in the generalized gradient approximation (GGA), following the Perdew-Burke-Ernzerhof

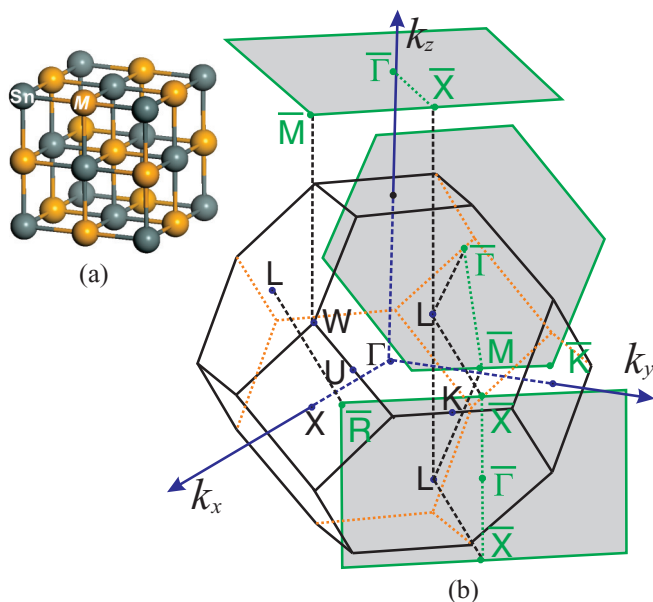


FIG. 1. (Color online) (a) SnM ($M = \text{S}$ and Se) rocksalt lattice structure and (b) face cubic centered (FCC) Brillouin zone (BZ). Two dimensional BZ projected onto the (001), (110), and (111) surfaces are also shown in (b). These three surfaces are all perpendicular to the $(\bar{1}10)$ mirror symmetry plane.

parametrization scheme,²⁰ with the projected augmented wave method as implemented in the Vienna *Ab initio* Simulation Package (VASP).^{21,22} The energy cutoff is set to be 500 eV. The TB matrix elements are calculated by projection onto maximally localized Wannier orbitals,^{23–25} using the VASP2WANNIER90 interface.²⁶

Early experimental characterizations^{27–29} have found that both SnS and SnSe crystallize in low temperatures at *Pnma* GeS-type orthorhombic phase³⁰ and that at high temperatures two metastable orthorhombic *Cmcm* TII-type³⁰ and *Fm $\bar{3}m$* rocksalt cubic NaCl-type phases²⁹ (Fig. 1) exist. Here, we focus on the rocksalt structure, which has been shown to be stable under epitaxial growth of SnSe and SnS on a NaCl substrate with lattice constants $a_{\text{Expt}}^{\text{SnSe}} = 5.99 \text{ \AA}$ ²⁸ and $a_{\text{Expt}}^{\text{SnS}} = 6.00 \text{ \AA}$ ²⁸ and 5.80 \AA ,³¹ respectively. Our first-principles calculations find that the optimized lattice constants are $a_{\text{Theo}}^{\text{SnSe}} = 6.05 \text{ \AA}$ and $a_{\text{Theo}}^{\text{SnS}} = 5.85 \text{ \AA}$ for SnSe and SnS, respectively, in good agreement with the experimental values.

Since very recent experiments have found orthorhombic SnS grown even on a NaCl substrate,³² with epitaxial growth conditions different from the ones in the previous reports,^{28,31} it is desirable to check the stability of the *Fm $\bar{3}m$* rocksalt

cubic phase with respect to the *Pnma* orthorhombic phase for both SnS and SnSe compounds. The total energy calculations using DFT with GGA find that the energy difference between the cubic and orthorhombic phases in bulk are very small. The *Pnma* orthorhombic phase is lower in energy only by 74 meV/unit cell and 0.78 meV/unit cell than the *Fm $\bar{3}m$* cubic phase for SnS and SnSe, respectively (see Table I). This result implies that the metastable *Fm $\bar{3}m$* cubic phase is thermodynamically accessible. It should be also noted here that the known rocksalt phase may have been misassigned as zincblende, as suggested recently by Burton and Walsh.³³

III. RESULTS

A. Bulk band structure

The calculated bulk band structures along the high symmetry lines around L in the Brillouin zone (BZ) are shown in Figs. 2(a)–2(d), and for comparison the results for those of the isostructural TCI SnTe are also plotted in Figs. 2(e) and 2(f).^{5,7} The band structures of SnS, SnSe, and SnTe display similar features, which are summarized as follows: (i) Without SOC, all compounds have a gapless three-dimensional (3D) Dirac cone located in the vicinity of the high symmetry L point along the L - W line; (ii) level anticrossing occurs once SOC is included and the 3D Dirac cone is broken with opening a finite band gap; (iii) the top of the valence band and the bottom of the conduction band at and near L are primarily composed of Sn p -like and S/Se/Te p -like states, respectively; (iv) the parity of the top (bottom) of the valence (conduction) band at L is odd (even); (v) the band character around L remains unchanged upon including SOC. These features already indicate that rocksalt SnS and SnSe are TCIs just like SnTe.³⁶ It should be emphasized here that, unlike TIs,^{11–18} the inverted band order is found to be driven not by SOC but solely by chemical bonding and crystal field [see Fig. 3(b)].

The occurrence of band inversion at an even number of k points (i.e., four equivalent L points) and the fact that this band inversion is not driven by SOC are suggestive of the formation of a crystal-symmetry driven nontrivial topological state. In order to provide further support, let us study the evolution of the band gap as a function of the lattice constant. It is an obvious fact that any insulator is topologically trivial in the atomic limit. Therefore, the occurrence of inverted band order implies that the band gap has to close and reopen by progressively increasing the lattice constant. This behavior is indeed found in Fig. 3(a): The band gap E_g at L closes with increasing the lattice constant and then reopens with the opposite band character, i.e., the parity as well as the

TABLE I. Total energy difference ΔE between the *Pnma* orthorhombic (E_{ortho}) and *Fm $\bar{3}m$* rocksalt cubic (E_{cubic}) phases for SnS and SnSe with experimental and relaxed lattice constants. The *ab initio* DFT-GGA calculations with including SOC are employed. For comparison, the results for SnTe are also shown. The experimental lattice constants are taken from Ref. 28.

$\Delta E = E_{\text{ortho}} - E_{\text{cubic}}$ (eV/unit cell)					
SnS		SnSe		SnTe	
Experimental	Relaxed	Experimental	Relaxed	Experimental	Relaxed
-0.0600	-0.0743	0.151	-0.000782	0.504	0.0675

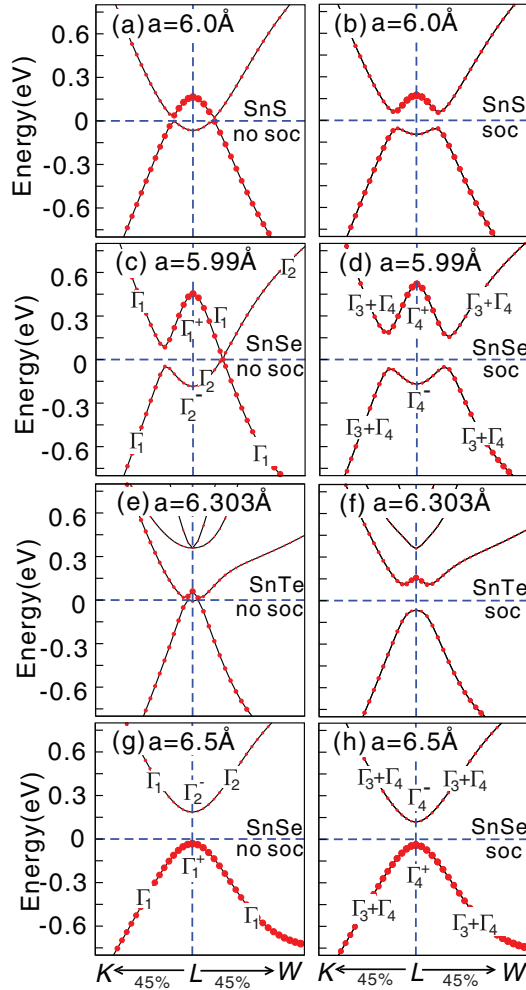


FIG. 2. (Color online) Electronic band structures obtained by first-principles calculations for SnS (a), (b), SnSe (c), (d), (g), (h), and SnTe (e), (f) with and without SOC. The size of red dots is proportional to the amount of contributing weight in each band from S (a), (b), Se (c), (d), (g), (h), or Te (e), (f) atoms. In (a)–(f), the experimental lattice constant a (indicated in the figures) is used,³⁴ whereas in (g) and (h) an expanded lattice constant is used. The irreducible representations of the bands closest to Fermi energy (set to be 0) are also indicated.³⁵ The regions of momentum taken in the horizontal axes are 45% of the L - K and L - W lines from L , as indicated in the figures.

main contributing weight of the constituent atoms being reversed for the top of the valence band and the bottom of the conduction band [Figs. 2(d) and 2(h)]. These results clearly demonstrate that a topological phase transition from a topologically nontrivial to a trivial state occurs with increasing the lattice constant. Note that a similar behavior is found even without including SOC [Figs. 2(c) and 2(g)], indicating that SOC has indeed no influence in determining the band character around L . The evolution of the band character is schematically drawn in Fig. 3(b).

To quantify the topological feature, we shall evaluate the mirror Chern number. We first calculate the Berry curvature $\Omega^m(\mathbf{k}) = \nabla_{\mathbf{k}} \times \mathbf{A}^m(\mathbf{k})$ on the $(\bar{1}10)$ mirror symmetry plane in the BZ. Here, $\mathbf{A}^m(\mathbf{k}) = i \sum_n \langle u_n^m(\mathbf{k}) | \nabla_{\mathbf{k}} | u_n^m(\mathbf{k}) \rangle$ is the Berry

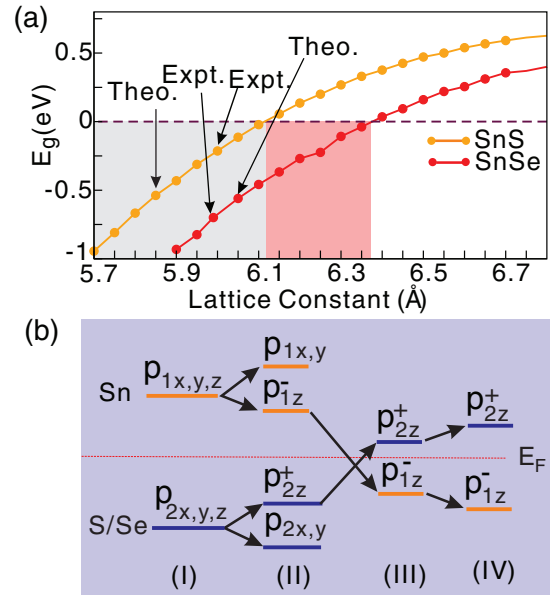


FIG. 3. (Color online) (a) The evolution of the band gap E_g calculated with SOC as a function of the lattice constants for SnS and SnSe. The energy gap E_g is defined as the energy difference between the top of the valence band and the bottom of the conduction band at L , i.e., $E_g = E_{-}^L - E_{+}^L$, where E_p^L is the band energy with parity p ($= +, -$) at L . Thus, E_g is negative when the bands are in inverted order. The optimized (Theo.) and experimental (Expt.) lattice constants are indicated by arrows, all located within the nontrivial topological region. (b) A schematic energy level diagram around L : (I) atomic limit, (II) including hybridization with a large lattice constant, (III) with the experimental lattice constant, and (IV) inclusion of SOC. The band is inverted already in (III) without SOC. Here E_F stands for Fermi energy. The signs ($+$, $-$) denote the parities of the corresponding p -like orbitals.

connection, $u_n^m(\mathbf{k})$ is the n th eigenstate at momentum \mathbf{k} and with mirror eigenvalue m ($= \pm i$) of the TB model described below, and the sum is over all occupied bands. The results of the component $\Omega_{\perp}^m(\mathbf{k})$ perpendicular to the $(\bar{1}10)$ mirror plane are shown in Fig. 4 for SnSe with both experimental and expanded lattice constants. We find that the main contributions are from momenta close to L and that $\Omega_{\perp}^{+i}(\mathbf{k}) = -\Omega_{\perp}^{-i}(\mathbf{k})$. We evaluate the mirror Chern number,³⁷ $c_M = (n_{+i} - n_{-i})/2$, where $n_m = \int \Omega^m(\mathbf{k}) \cdot dS$, and find that $c_M = -2$ (0) for SnSe with the experimental (expanded) lattice constant, confirming the topological transition from a TCI to a trivial insulator with increasing the lattice constant. We also calculate the Z_2 indices ($\nu_0; \nu_1 \nu_2 \nu_3$)³⁸ and find that this index is (0; 000) (see Fig. 5) for SnSe with both experimental and expanded lattice constants, suggesting that they are not time-reversal Z_2 TIs.

B. Surface band structure

Let us next examine the intrinsic properties of the topological phase in SnS and SnSe, and provide further evidence of this TCI state by inspecting the surface properties. Unlike TIs for which an odd number of Dirac cones appears in any surface orientation, TCIs have an even number of topologically protected Dirac cones on high symmetry surfaces. For the rocksalt crystal structure, gapless surface states are expected

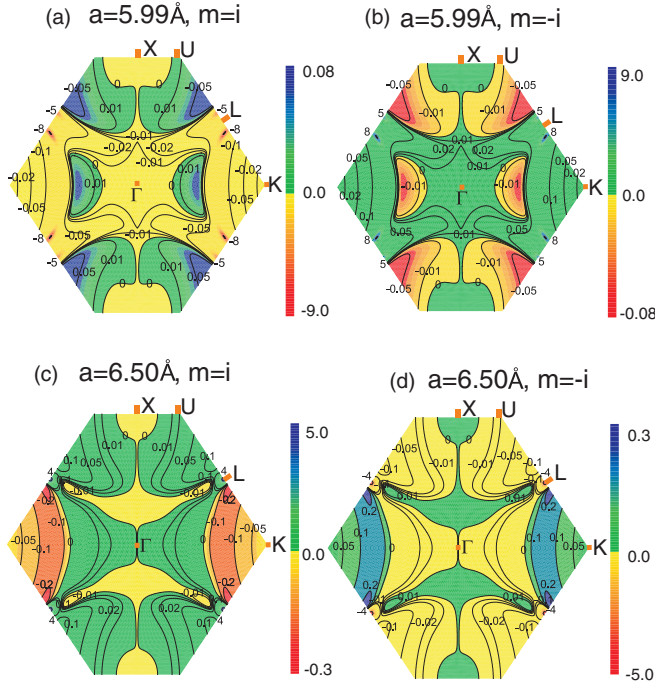


FIG. 4. (Color online) Contour plots of the Berry curvature $\Omega^m(\mathbf{k})$ on the $(\bar{1}10)$ mirror symmetry plane in the BZ for SnSe with the experimental lattice constant $a = 5.99 \text{ \AA}$ (a), (b) and with an expanded lattice constant $a = 6.5 \text{ \AA}$ (c), (d). Only the component $\Omega_{\perp}^m(\mathbf{k})$ perpendicular to the $(\bar{1}10)$ mirror plane with $m = \pm i$ is plotted. Notice that $\Omega_{\perp}^{+i}(\mathbf{k}) = -\Omega_{\perp}^{-i}(\mathbf{k})$. The high symmetry momenta, $\mathbf{k} = n_1 \mathbf{b}_1/2 + n_2 \mathbf{b}_2/2 + n_3 \mathbf{b}_3/2$, are indicated by $\Gamma : (n_1, n_2, n_3) = (0, 0, 0)$, $X : (1, 1, 0)$, $U : (\frac{5}{4}, \frac{5}{4}, \frac{1}{2})$, $L : (1, 1, 1)$, and $K : (\frac{3}{4}, \frac{3}{4}, \frac{3}{2})$ with the reciprocal lattice vectors $\mathbf{b}_1 = \frac{2\pi}{a}(-1, 1, 1)$, $\mathbf{b}_2 = \frac{2\pi}{a}(1, -1, 1)$, and $\mathbf{b}_3 = \frac{2\pi}{a}(1, 1, -1)$.

to exist only on surfaces that are perpendicular to the $(\bar{1}10)$ mirror symmetry plane (and the symmetrically equivalent planes).^{5,9,39}

To prove these expectations, we shall now compute the band dispersions for the (001), (110), and (111) surfaces [see Fig. 1(b)] using the *ab initio* TB model. The *ab initio* TB model is constructed by downfolding the bulk energy bands, obtained by first-principles calculations, using maximally localized Wannier functions (MLWFs). As the bulk energy bands near Fermi energy are predominantly formed by hybridized *p*-like

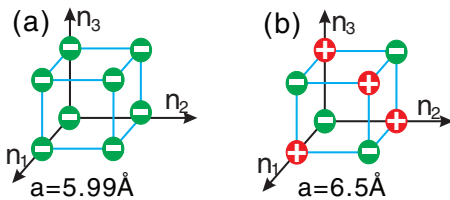


FIG. 5. (Color online) The products $(\delta_{n_1 n_2 n_3} = \pm 1)$ of parity eigenvalues from the occupied states at eight time-reversal invariant momenta \mathbf{k} , i.e., $n_1, n_2, n_3 = 0, 1$, are indicated by \pm for SnSe with both experimental (a) and expanded (b) lattice constants. Here $\mathbf{k} = n_1 \mathbf{b}_1/2 + n_2 \mathbf{b}_2/2 + n_3 \mathbf{b}_3/2$ and the definition of \mathbf{b}_i ($i = 1, 2, 3$) is given in Fig. 4.

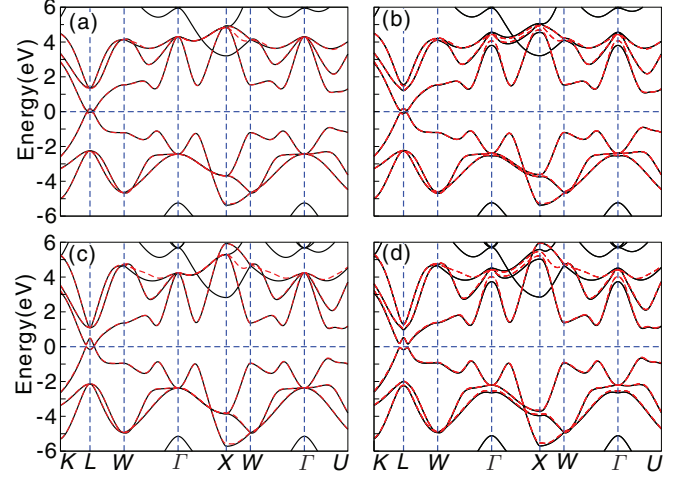


FIG. 6. (Color online) Comparison of the bulk energy band structures obtained from the *ab initio* TB model (red dashed lines) and from the first-principles DFT calculations (black solid lines) for rocksalt SnS (a), (b) and SnSe (c), (d). Figures (a), (c) and (b), (d) correspond to the cases without and with including SOC, respectively. The Fermi energy E_F is set to be 0.

Sn and S/Se orbitals, the MLWFs are derived from atomic *p*-like orbitals and the TB parameters are determined from the MLWFs overlap matrix. The SOC is considered here in the atomic form:

$$H_{\text{SO}}^p(\lambda) = \frac{\lambda}{2} \begin{bmatrix} 0 & 0 & -i & 0 & 0 & 1 \\ 0 & 0 & 0 & i & -1 & 0 \\ 0 & -i & 0 & 0 & 0 & -i \\ 0 & -1 & 0 & i & 0 & 0 \\ 1 & 0 & i & 0 & 0 & 0 \end{bmatrix} \quad (1)$$

with *p*-like orbital bases $\{|p_x, \uparrow\rangle, |p_x, \downarrow\rangle, |p_y, \uparrow\rangle, |p_y, \downarrow\rangle, |p_z, \uparrow\rangle, |p_z, \downarrow\rangle\}$, where arrows indicate electron spins. The SOC parameter λ for Sn, Se, and S are taken from experimental spectral data, i.e., $\lambda_{\text{Sn}} = 0.27 \text{ eV}$, $\lambda_{\text{Se}} = 0.22 \text{ eV}$, and $\lambda_{\text{S}} = 0.05 \text{ eV}$, respectively.⁴⁰ The quality of the TB parametrization is successfully assessed in Fig. 6, where the TB bulk band structures are compared with the corresponding first-principles DFT results.

It is clearly seen in Fig. 6 that the TB bulk bands perfectly reproduce the DFT bands around the Fermi energy E_F up to $\sim \pm 3 \text{ eV}$. It is also noticed that, in energy regions above and below $\sim 3 \text{ eV}$ from E_F , the TB bands deviate slightly from the DFT bands. This deviation is simply understood because the bands in the high (low) energy region above $\sim 3 \text{ eV}$ (below $\sim -3 \text{ eV}$) are contributed also by *d*-like (*s*-like) orbitals, which are not included in the TB model. However, this does not degrade the present TB parametrization since we focus on the energy region close to E_F (see Figs. 2 and 7). It should be also emphasized that the TB model reproduces all the band symmetries correctly, which is essential to determine the topological properties of the systems.

Encouraged by this quantitative agreement, let us finally compute the surface band structures by adopting three slabs for the (001), (110), and (111) surfaces with thickness of 89, 89, and 239 atomic layers, respectively. The results of

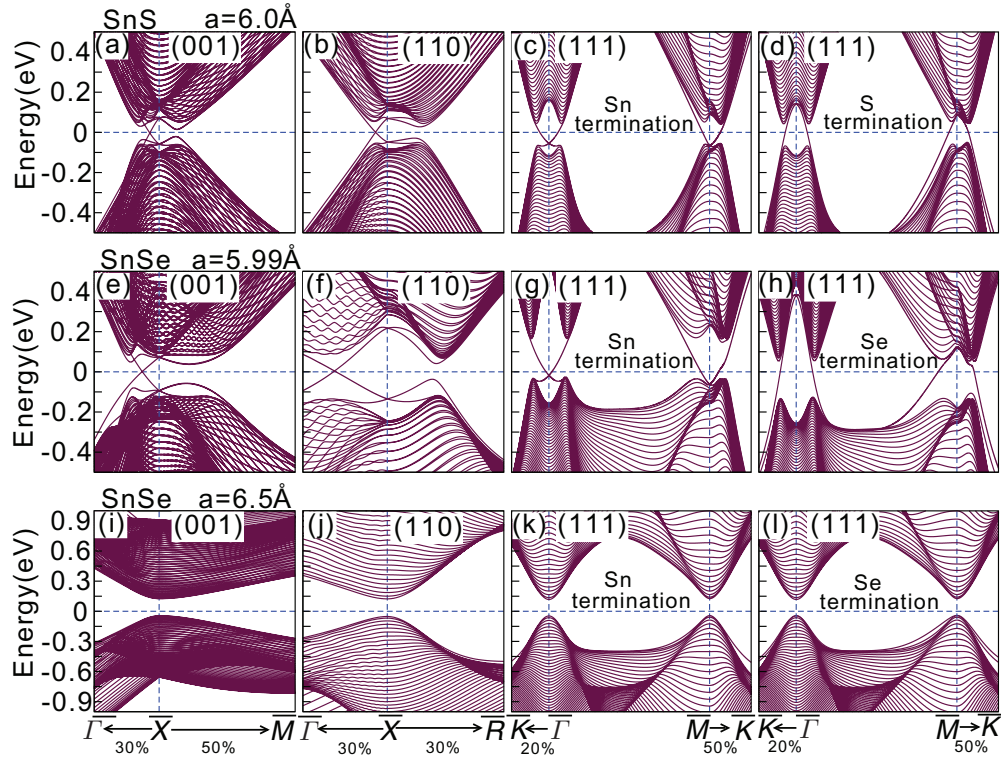


FIG. 7. (Color online) TB energy band structures of the (001), (110), and (111) surfaces for rocksalt (a)–(d) SnS with the experimental lattice constant $a = 6.0 \text{ \AA}$, (e)–(h) SnSe with the experimental lattice constant $a = 5.99 \text{ \AA}$, and (i)–(l) SnSe with an expanded lattice constant $a = 6.5 \text{ \AA}$. Notice that there exist two distinct surface terminations for the (111) surface. In (a)–(h) the appearance of the gapless Dirac-cone-like metallic states evidences the occurrence of TCI. With expanding the lattice constant in (i)–(l), the Dirac-cone-like metallic surface states disappear, suggesting that the system is a trivial insulator. The surface projected momenta are indicated in Fig. 1(b). The Fermi energy E_F is set to be 0. The regions of momentum taken in the horizontal axes along the high symmetry lines are also indicated.

the TB calculations are summarized in Fig. 7. These results show clearly that the (001), (110), and (111) surfaces with the experimental lattice constants possess metallic states with opposite mirror eigenvalues, which cross each other forming a massless Dirac cone. It has been shown^{5,9} that the rocksalt TCIs with the mirror Chern number $c_M = -2$ guarantees the presence of two pairs of counterpropagating, spin-resolved surface states with opposite mirror eigenvalues along all symmetrically equivalent $\bar{\Gamma}$ - \bar{X} lines in the (001) surface, and only one pair in the (110) surface [Fig. 1(b)]. Indeed, both SnS and SnSe surfaces follow this symmetry consideration, displaying four equivalent Dirac cones in the (001) surface [Figs. 7(a) and 7(e)] and two Dirac cones in the (110) surface [Figs. 7(b) and 7(f)]. Instead, similarly to the case of SnTe,⁹ four Dirac cones are found in the (111) surface, one at $\bar{\Gamma}$ and other three at \bar{M} , as shown in Figs. 7(c), 7(d), 7(g), and 7(h).

In addition, as already shown in Figs. 3(a) and 4, for the lattice constants larger than 6.10 \AA for SnS and 6.37 \AA for SnSe, the band character changes and the systems undergo a topological transition towards a trivial insulator. This is clearly reflected also in the surface band structures computed for SnSe with the lattice constant $a = 6.50 \text{ \AA}$ in Figs. 7(i)–7(l): the Dirac cones disappear and a broad spectral feature develops on the top (bottom) of the valence (conduction) band with a finite band gap, a typical behavior of an ordinary trivial insulator.

These results unambiguously demonstrate that rocksalt SnS and SnSe represent the features of TCI.

IV. CONCLUSIONS

Using first-principles calculations together with *ab initio* tight-binding model analyses, we have revealed that rocksalt SnS and SnSe represent a prime example of topological crystalline insulators at ambient pressure without incorporating heavy elements. We have shown that in both systems an even number of symmetry-protected Dirac cones emerge in the (001), (110), and (111) surfaces perpendicular to the $(\bar{1}10)$ mirror symmetry plane. We have also shown that the spin-orbit coupling is still important to open the band gap in the bulk phases although it is not necessary to drive the topologically nontrivial state with the inverted band order, as proposed in the original theory.³ We have also demonstrated that a topological transition occurs toward a trivial insulator upon volume expansion. Finally, we emphasize that the onset of the topological crystalline insulating state in SnS and SnSe is not dependent on alloying, strain, pressure, or any electronic structure engineering, but SnS and SnSe are both topological crystalline insulators in their native phase.

Although the bulk ground state of both SnS and SnSe is in $Pnma$ orthorhombic phase, we have shown that the energy difference between the ground state and the $Fm\bar{3}m$

cubic rocksalt phase is very small. This clearly suggests that the rocksalt phase is certainly experimentally accessible, stimulating further experimental efforts in this direction.

ACKNOWLEDGMENTS

This work was supported by the “Hundred Talents Project” of the Chinese Academy of Sciences, NSFC of China (Grants

No. 51074151 and No. 51174188), Grant-in-Aid for Scientific Research from MEXT Japan (Grants No. 24740269 and No. 25287096), and the RIKEN iTHES Project. We acknowledge the Vienna Scientific Cluster, the Beijing Supercomputing Center of CAS (including in Shenyang branch), and the RIKEN Cluster of Clusters (RICC) facility for computational resources. Y.S. has been supported by the International Program Associate (IPA) program in RIKEN.

*Corresponding author: xingqiu.chen@imr.ac.cn

¹M. Z. Hasan and C. L. Kane, *Rev. Mod. Phys.* **82**, 3045 (2010).

²X. L. Qi and S. C. Zhang, *Rev. Mod. Phys.* **83**, 1057 (2011).

³L. Fu, *Phys. Rev. Lett.* **106**, 106802 (2011).

⁴Also see R.-J. Slager, A. Mesaros, V. Jurić, and J. Zaanen, *Nature Phys.* **9**, 98 (2013).

⁵T. H. Hsieh, H. Lin, J. Liu, W. Duan, A. Bansil, and L. Fu, *Nature Commun.* **3**, 982 (2012).

⁶P. Dziawa, B. J. Kowalski, K. Dybko, R. Buczko, A. Szczerbakow, M. Szot, E. Lusakowska, T. Balasubramanian, B. M. Wojek, M. H. Berntsen, O. Tjernberg, and T. Story, *Nature Mater.* **11**, 1023 (2012).

⁷Y. Tanaka, Z. Ren, T. Sato, K. Nakayama, S. Souma, T. Takahashi, K. Segawa, and Y. Ando, *Nature Phys.* **8**, 800 (2012).

⁸S. Y. Xu, C. Liu, N. Alidoust, D. Qian, M. Neupane, J. D. Denlinger, Y. J. Wang, H. Lin, L. A. Wray, R. J. Cava, A. Marcinkova, E. Morosan, A. Bansil, and M. Z. Hasan, *Nature Commun.* **3**, 1192 (2012).

⁹J. Liu, W. Duan, and L. Fu, [arXiv:1304.0430](https://arxiv.org/abs/1304.0430).

¹⁰P. Barone, T. Rauch, D. DiSante, J. Henk, I. Mertig, and S. Picozzi, *Phys. Rev. B* **88**, 045207 (2013); P. Barone, D. DiSante, and S. Picozzi, *Phys. Status Solidi RRL* **7**, 1102 (2013).

¹¹Y. Xia, D. Qian, D. Hsieh, L. Wray, A. Pal, H. Lin, A. Bansil, D. Grauer, Y. S. Hor, R. J. Cava, and M. Z. Hasan, *Nature Phys.* **5**, 398 (2009).

¹²H. Zhang, C.-X. Liu, X.-L. Qi, X. Dai, Z. Fang, and S.-C. Zhang, *Nature Phys.* **5**, 438 (2009); C. X. Liu, X. L. Qi, H. J. Zhang, X. Dai, Z. Fang, and S. C. Zhang, *Phys. Rev. B* **82**, 045122 (2010).

¹³H. Z. Lu, W. Y. Shan, W. Yao, Q. Niu, and S. Q. Shen, *Phys. Rev. B* **81**, 115407 (2010).

¹⁴J. G. Analytis, J. H. Chu, Y. Chen, F. Corredor, R. D. McDonald, Z. X. Shen, and I. R. Fisher, *Phys. Rev. B* **81**, 205407 (2010).

¹⁵D. Xiao, Y. Yao, W. Feng, J. Wen, W. Zhu, X.-Q. Chen, G. M. Stocks, and Z. Zhang, *Phys. Rev. Lett.* **105**, 096404 (2010).

¹⁶Y. Sun, X.-Q. Chen, S. Yunoki, D. Li, and Y. Li, *Phys. Rev. Lett.* **105**, 216406 (2010).

¹⁷Y. Sun, X.-Q. Chen, C. Franchini, D. Li, S. Yunoki, Y. Li, and Z. Fang, *Phys. Rev. B* **84**, 165127 (2011).

¹⁸Y. Chen, *Front. Phys.* **7**, 175 (2012).

¹⁹M. Kargarian and G. A. Fiete, *Phys. Rev. Lett.* **110**, 156403 (2013).

²⁰J. P. Perdew, K. Burke, and M. Ernzerhof, *Phys. Rev. Lett.* **77**, 3865 (1996).

²¹G. Kresse and J. Hafner, *Phys. Rev. B* **48**, 13115 (1993).

²²G. Kresse and J. Furthmüller, *Comput. Mater. Sci.* **6**, 15 (1996).

²³N. Marzari and D. Vanderbilt, *Phys. Rev. B* **56**, 12847 (1997).

²⁴I. Souza, N. Marzari, and D. Vanderbilt, *Phys. Rev. B* **65**, 035109 (2001).

²⁵A. A. Mostofi, J. R. Yates, Y. S. Lee, I. Souza, D. Vanderbilt, and N. Marzari, *Comput. Phys. Commun.* **178**, 685 (2008).

²⁶C. Franchini, R. Kovik, M. Marsman, S. S. Murthy, J. He, C. Ederer, and G. Kresse, *J. Phys.: Condens. Matter* **24**, 235602 (2012).

²⁷P. M. Nikolic, *Br. J. Appl. Phys.* **16**, 1075 (1965).

²⁸A. N. Mariano and K. L. Chopra, *Appl. Phys. Lett.* **10**, 282 (1967).

²⁹L. S. Palatnik and V. V. Levitin, *Dokl. Akad. Nauk SSSR* **96**, 975 (1954).

³⁰T. Chattopadhyay, J. Pannetier, and H. G. Von Schnering, *J. Phys. Chem. Solids* **47**, 879 (1986).

³¹B. F. Bilenkii, A. G. Mikolaichuk, and D. M. Freik, *Phys. Status Solidi* **28**, K5 (1968).

³²A. Wangperawong, S. M. Herron, R. R. Runser, C. Häggglund, J. T. Tanskanen, H. B. R. Lee, B. M. Clemens, and S. F. Bent, *Appl. Phys. Lett.* **103**, 052105 (2013).

³³L. A. Burton and A. Walsh, *J. Phys. Chem. C* **116**, 24262 (2012).

³⁴The experimental lattice constant of SnTe is taken from Ref. 28.

³⁵Although not shown for clarity, the same irreducible representations are assigned to the bands of SnS and SnTe. Note that the origin of the symmetry operations is set to Sn atom.

³⁶One of the important quantitative differences is that the band gap \mathcal{E}_g of SnSe ($\mathcal{E}_g \sim 0.202$ eV) seems larger than SnTe ($\mathcal{E}_g \sim 0.172$ eV). However, more careful study beyond GGA is required for better quantitative comparison.

³⁷J. C. Y. Teo, L. Fu, and C. L. Kane, *Phys. Rev. B* **78**, 045426 (2008).

³⁸L. Fu, C. L. Kane, and E. J. Mele, *Phys. Rev. Lett.* **98**, 106803 (2007).

³⁹S. Safaei, P. Kacman, and R. Buczko, *Phys. Rev. B* **88**, 045305 (2013).

⁴⁰K. Wittel and R. Manne, *Theor. Chim. Acta* **33**, 347 (1974).